fortune Journals

Research Article

INTERNATIONAL
JOURNAL OF APPLIED BIOLOGY AND PHARMACEUTICAL TECHNOLOGY
ISSN: 0976-4550

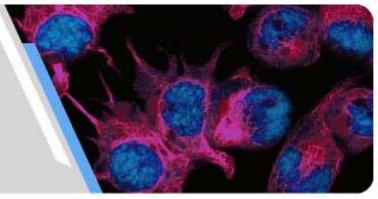

Intelligent Syringe for Porous Tissue Characterization Using Advanced Darcy Flow Pressure Transient Analysis

Wilson C. Chin[1*], Jamie A. Chin[2] and Xiaoying Zhuang[1]

Abstract

An instrumented "intelligent syringe" for tissue properties prediction is described. The syringe records pressure transients created while injecting or withdrawing fluid from tissue at given flow rates. Dynamic data is interpreted using computer-based porous media math models to predict permeability, anisotropy, compressibility, background pressure and porosity. The new method provides direct measurements of flow properties important to drug delivery, clinical diagnosis, disease control, synthetic organ design and research endeavors. The approach conveniently, rapidly and inexpensively supplements conventional methods like X-ray, Catscan, MRI and ultrasound, which offer qualitative results through gray scale images requiring physician dependent and subjective analysis. The "*i*Syringe" supports portable target monitoring on daily or weekly bases; it provides local quantitative information useful in understanding global qualitative results obtained from traditional methods. The theoretical foundations of the method are derived, validated mathematically, and applied to published human and animal data, highlighting potential clinical and research applications.

Keywords: Catscan, compressibility, medical imaging, MRI, permeability, syringe, tissue properties, tumor growth, ultrasound, X-ray.

Introduction

Conventional imaging methods like X-ray, Catscan, MRI and ultrasound, which have revolutionized medical diagnosis, provide only qualitative information useful in identifying local anomalies. Such methods can be inconvenient, time-consuming and expensive, and cannot be routinely used in doctors' offices. Conclusions depend on physician expertise and experience, not to mention patient sex, health, age and ethnicity. They are highly subjective. Very often, additional quantitative information over smaller spatial scales is needed for detailed evaluation. Resulting treatment strategies may require active monitoring of tissue properties on a periodic basis.

We introduce the "intelligent syringe," or "iSyringe," a new imaging device that is inexpensive, convenient, offering detailed information extracted from syringe data based on exact analytical solutions to Darcy flow formulations. Digitized pressure transient traces are recorded at locations within the syringe body or needle, and possibly along the external needle surface. These are interrogated using special "inverse solutions" to provide estimates for local permeability, anisotropy, compressibility, background pressure and porosity. Data collection times are 10-20 seconds, an interval within the range of typical injections or withdrawals. Optimal time window durations needed to acquire multiple "time, pressure" values accurately are controlled by adjusting a mechanism within the syringe system. Aside

Affiliation:

[1]Research and Development, Stratamagnetic Software, LLC, Houston, Texas, USA

[2]University of Hong Kong, Hong Kong, China

Corresponding Author:
Wilson C. Chin, Ph.D., M.I.T., Research and Development, Stratamagnetic Software, LLC, Houston, Texas, USA.
URL: www.stratamagnetic.com.
Email: stratamagnetic.software@outlook.com.
Mobile phone: (832) 483-6899.

Citation: Wilson C. Chin, Jamie A. Chin and Xiaoying Zhuang. Intelligent Syringe for Porous Tissue Characterization Using Advanced Darcy Flow Pressure Transient Analysis. International Journal of Applied Biology and Pharmaceutical Technology. 15 (2024): 24-39.

Received: September 20, 2024
Accepted: September 25, 2024
Published: October 16, 2024

from instrumentation and automated analysis, the predictive process is transparent to the patient and requires minimal supervision and operational expertise.

Methods for Pressure Interpretation

Theoretical Considerations

Blood and injectate tissue flows represent low Reynolds number phenomena satisfying mathematical Darcy formulations. Permeability measures the resistance a tissue sample offers to fluid motion; the lower the permeability, the higher the resistance, and vice-versa. Low values may impede circulation while higher values may indicate swelling. Simple one-dimensional lab tests are often used to determine permeability for animal tissues using the formula "$Q = Ak/\mu\ \Delta P/L$," where Q is volume flow rate, A is flow area, k is permeability, μ is Newtonian viscosity, ΔP is pressure drop and L is thickness. Despite the apparent simplicity, this approach requires actual and inconvenient liquid transport through tissue. This contrasts with indirect pressure transfer associated with compressibility changes within the medium, for example, sound waves propagating through solids or coupled transport and diffusion in porous tissue.

Not only are "$Q = Ak/\mu\ \Delta P/L$" procedures costly and time-consuming – since they cannot be performed on live specimens, they are not useful in diagnostic evaluation and are relegated to post-mortem exams. We consider transient pressure diffusion processes in porous media. In particular, we formulate and solve "forward" and "inverse" problems for Darcy flow in transversely isotropic porous tissue. A minimally invasive alternative to the laboratory procedure described is developed. Dynamic syringe pressure data collected during withdrawal and injection contain significant tissue properties information. These attributes, obtained by interrogating measured "pressure versus time" curves using special algorithms, may shed quantitative insights into local physical anomalies. We first summarize exact analytical solutions to "forward models," and then present complementary "inverse solutions" for tissue properties. Mathematical validations are offered, and applications to human and swine data are given demonstrating potential clinical uses.

Transient *Isotropic* Darcy Flow – Forward Solutions for Liquids

If P(r,t) denotes Darcy pressure in an isotropic medium with permeability k, porosity φ, compressibility c and Newtonian viscosity μ, the governing equation satisfies $\partial^2 P(r,t)/\partial r^2 + 2/r\ \partial P/\partial r = (\varphi\mu c/k)\ \partial P/\partial t$ where r is the spherical radius and t is time. We invoke the initial condition $P(r,t=0) = P_0$, the farfield condition $P(r=\infty,t) = P_0$ and the syringe constraint $(4\pi R_w^2 k/\mu)\ \partial P(R_w,t)/\partial r - VC\ \partial P/\partial t = Q(t)$. Here, P_0 describes tissue pressure far from the needle contact, while $r = R_w$ represents the effective radius for a control surface surrounding that point. This is not precisely known since needles may end abruptly or with beveled angles. A multiplicative geometric correction factor *G*, suggesting "$r = GR_w$," is introduced where *G* is determined empirically. Here, we assume $G = 1$ for simplicity.

The differential equation describes mass conservation, while the syringe constraint describes volume effects at the contact. For example, $(4\pi R_w^2 k/\mu)\ \partial P(R_w,t)/\partial r = Q(t)$ states that the velocity $(k/\mu)\ \partial P(R_w,t)/\partial r$ and surface area $4\pi R_w^2$ product must equal the volume flow rate Q(t). In general, this is not true since the needle connects to a syringe volume V containing fluid with compressibility C. Here $VC\ \partial P/\partial t$ describes "cushioning effects" that model flowline fluid expansion and decompression, which affect time scales associated with syringe actions. VC can be adjusted to change the time window available for data acquisition, e.g., decreased to reduce times for steady-state pressures or increased to lengthen times for more careful transient pressure collection. The analytical, closed form, exact solution to our initial-boundary value problem is solved as follows.

We introduce *italicized* dimensionless variables $r = r/r^*$, $t = t/t^*$, $p(r,t) = \{P(r,t) - P_0\}/p^*$ and $Q(t) = Q_0\ F(t)$, requiring $r^* = VC/(4\pi R_w^2 \varphi c)$, $t^* = V^2C^2\mu/(16\pi^2 R_w^4\ k\varphi c)$ and $p^* = VCQ_0\mu/(16\pi^2 R_w^4\ k\varphi c)$. Here Q_0 is a positive or negative and a dimensionless $F(t)$ is given. For continuous constant flow rates, $F(t)$ is unity; for piecewise-constant multi-rate pumping, $F(t)$ is represented by a sequence of step functions. We take $Q(t) = Q_0\ F(t) = Q_0$ and $F(t) = 1$ for constant rates, with $Q_0 > 0$ for withdrawal and $Q_0 < 0$ for injection. The problem reduces to a dimensionless form containing a sole parameter r_w with $\partial^2 p(r,t)/\partial r^2 + 2/r\ \partial p/\partial r = \partial p/\partial t$, $p(r,0) = 0$, $p(\infty,t) = 0$ and $\partial p(r_w,t)/\partial r - \partial p/\partial t = F(t)$.

The dimensionless radius is $r_w = 4\pi R_w^3 \varphi c/(VC)$. Laplace transforms are used to develop an exact solution $p(r,t)$. If we define *complex* constants β_1 and β_2 with $\beta_1 = +\ 1/2 - 1/2\ \sqrt{(1 - 4\ r_w^{-1})}$ and $\beta_2 = +\ 1/2 + 1/2\ \sqrt{(1 - 4\ r_w^{-1})}$, the exact dimensionless source pressure for all time assuming F = 1 is

$$p_{exact}\ (r_w,t) = \{1/(\beta_1 - \beta_2)\}\{\beta_1^{-1} - \beta_1^{-1}\exp(\beta_1^2 t)\ \mathrm{erfc}(\beta_1\sqrt{t}) - \beta_2^{-1} + \beta_2^{-1}\exp(\beta_2^2 t)\ \mathrm{erfc}(\beta_2\sqrt{t})\} \quad (1a)$$

Exact solutions for $r > r_w$ are also available. The function $p_{exact}\ (r_w,t)$ also appears in the transversely isotropic problem addressed later. Here, "erfc" denotes the "complex complementary error function" with complex arguments [1]. In dimensional variables, the physical pressure becomes $P(r,t) = P_0 + p^* p(r,t)$ where p^*, *r* and *t* are defined previously. This can be simplified in certain limits. Taylor series expansions lead to early−time solutions, while asymptotic expansions yield later−time solutions, or

$$P(R_w,t)_{early\text{-}time} \approx P_0 - Q_0\ t/(VC) \quad (1b)$$

$$P(R_w,t)_{late\text{-}time} \approx P_0 - Q_0\ \mu/(4\pi R_w k) + \{Q_0\ \mu/(4\pi k)\}\sqrt{\{\varphi\mu c/(\pi k t)\}} \quad (1c)$$

The result for $P(R_w,t)$ at "early to intermediate times" is obtained using $e^t \approx 1 + t + t^2/2! + t^3/3! + \ldots$ and $\text{erfc}(z) \approx 1 - 2\pi^{-1/2} \exp(-z^2) \Sigma\, 2^n z^{2n+1}/\{(1)(3) \ldots (2n+1)\}$ with the summation taken over $(0,\infty)$. Expansions using rational polynomial functionals are also possible [1]. The resulting expressions, used for inverse analysis, enable straightforward properties predictions.

These results apply to constant rates. In practice, it may not be possible to control speeds accurately, resulting in variable rates. Sometimes sequences of different rates are used to perform multiple tests. Convolution integrals can be used to obtain solutions. If a constant rate solution is available, a variable rate solution is possible through superposition. In the analytical model, we assume a constant plunger speed with F = 1. For general F = F(τ), the dimensionless pressure would be

$$p_{exact}(r_w,t) = \{1/(\beta_1 - \beta_2)\} \times$$

$$\int_0^t F(\tau)\{\beta_2 \exp(\beta_2^2(t-\tau))\,\text{erfc}\,\beta_2\sqrt{(t-\tau)} - \beta_1 \exp(\beta_1^2(t-\tau))\,\text{erfc}\,\beta_1\sqrt{(t-\tau)}\}\,d\tau \quad (1d)$$

If F(τ) consists of piece−wise constant rates, solutions are expressible analytically. Continuous syringe withdrawals (or "drawdown" with pressure decreasing) or injections (or "buildup" with pressure increasing) satisfy single rate solutions. When these are terminated after finite time, formulas are constructed by superposing pressure solutions with reversed rate signs and corresponding time shifts. Such solutions are used to study the drawdowns and buildups in Figure 1.

Transient *Transversely Isotropic* Darcy Flow – Forward Solutions for Liquids

We have considered isotropic media where "r" is the spherical radius. The formulation implies spherically symmetric pressures because preferred directions do not appear. For transversely isotropic applications underlying many tissue flows, the equations differ. Two permeabilities are identical in a horizontal plane equal to k_h. A third value describes a vertical permeability k_v perpendicular to this reference plane. The more general partial differential equation and velocity flux models are

$$k_h\{\partial^2 P(x,y,z,t)/\partial x^2 + \partial^2 P(x,y,z,t)/\partial y^2\} + k_v\,\partial^2 P(x,y,z,t)/\partial z^2 = (\varphi\mu c)\,\partial P/\partial t \quad (2a)$$

$$P(x,y,z,t=0) = P_0 \quad (2b)$$

$$P(\sqrt{(x^2+y^2+z^2)} \to \infty, t) = P_0 \quad (2c)$$

$$\int \mathbf{q}\bullet\mathbf{n}\,dS - VC\,\partial P/\partial t = Q(t) \quad (2d)$$

Again k_h is the horizontal permeability in the x and y directions, while k_v is the vertical permeability along the z coordinate. These local Cartesian axes refer to target volume and not ground fixed coordinates. The k_h and k_v quantities in Figure 2 define a dip angle δ that vanishes when syringe and vertical axes coincide.

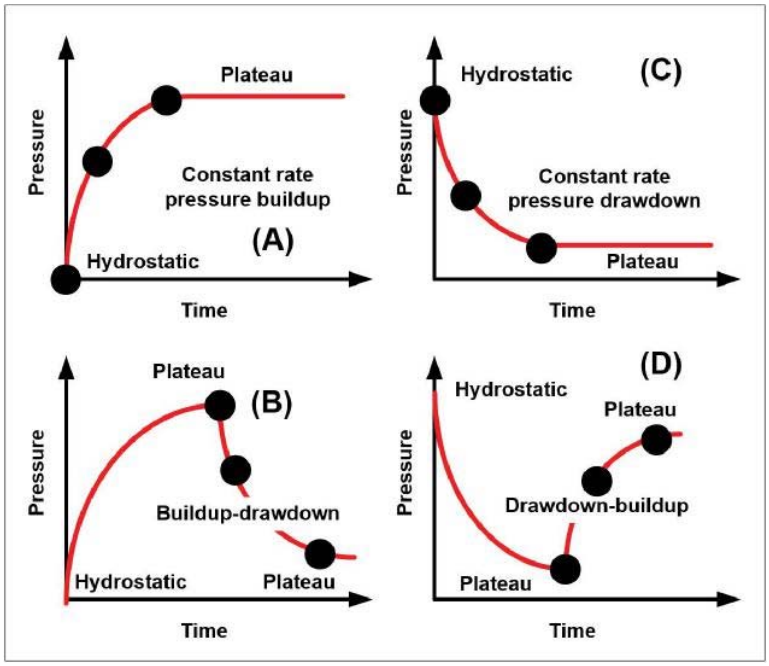

Figure 1. Transient pressure versus time curves at tissue contact. Black circles denote data acquisition points within drawdown or buildup cycles shown (three needed per cycle).

Wilson C. Chin et al., Int J Appl Biol Pharm 2024
DOI:10.26502/ijabpt.202132

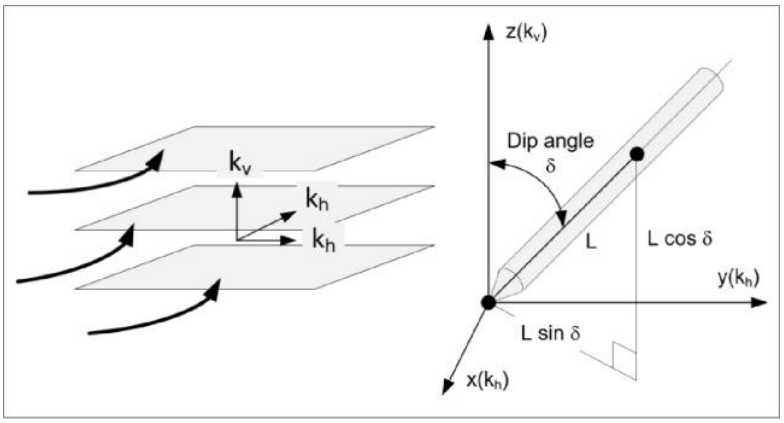

Figure 2. Local coordinates for transversely isotropic media, needle axis oriented at δ inclination relative to vertical permeability axis. Syringe body, plunger, control unit, infusion pump or auto-injector not shown. Continuous constant flow rate with and without stoppage studied in this paper.

Equation 2a represents mass conservation in transversely isotropic media. Syringe, needle and tissue interactions are described by Equation 2d where a closed integral over a control surface S surrounding the nozzle is shown. The integrand **q•n** denotes perpendicular components of the Darcy velocity **q** acting on S. This leads to $(4\pi R_w^2 k/\mu)\ \partial P(R_w,t)/\partial r$ in isotropic formulations when spherical symmetry applies and S is $4\pi R^2$. We now define dimensionless "starred" quantities $p^*(r^*,t^*) = \{P(x,y,z,t) - P_0\}/P_{ref}$ with $r^* = \{x^2/k_h + y^2/k_h + z^2/k_v\}^{1/2}$ and $t^* = t/t_{ref}$ so that $\partial^2 p^*/\partial r^{*2} + 2/r^* \partial p^*/\partial r^* = \phi\mu c/t_{ref}\ \partial p^*/\partial t^*$. Recall the spherical surface "$x^2 + y^2 + z^2 = R^2$" in the isotropic limit where R_w is a spherical well radius. Here we introduce an ellipsoidal surface $x^2/k_h + y^2/k_h + z^2/k_v\}^{1/2} = r^{*2}_w$ with a dimensionless $r^*_w = R_w/(k_h^{1/3}k_v^{1/6})$. It can be shown that $\int_\Sigma \mathbf{q} \bullet \mathbf{n}\ dS = -(4\pi r^{*2}_w P_{ref} k_v^{1/2} k_h/\mu)\ (\partial p^*/\partial r^*)_w$ so that $\partial^2 p^*/\partial r^{*2} + 2/r^*\ \partial p^*/\partial r^* = \phi\mu c/t_{ref}\ \partial p^*/\partial t^*$, $p^*(r^*,0) = 0$, $p^*(r^* \to \infty, t^*) = 0$, and finally $(4\pi r^{*2}_w P_{ref} k_v^{1/2} k_h/\mu)\ (\partial p^*/\partial r^*)_w - VCP_{ref}/t_{ref}\ \partial p^*/\partial t^* = Q_0 F(t^*)$.

We choose t_{ref} and P_{ref} to normalize the problem so it contains a single parameter. This is obtained using a second set of dimensionless *italicized* variables, taking $p^*(r^*,t^*) = p(r,t)$, $r = ar^*$ and $t = t^*$ where a is dimensionless. The choices $a = 4\pi\phi c k_v^{1/2} k_h r^{*2}_w/(VC)$, $t_{ref} = \mu V^2 C^2/(16\pi^2 \phi c k_v k_h^2 r^{*4}_w)$ and $P_{ref} = \mu Q_0 VC/(16\pi^2 \phi c k_v k_h^2 r^{*4}_w)$ reduce the problem to $\partial^2 p/\partial r^2 + 2/r\ \partial p/\partial r = \partial p/\partial t$, $p(r,t=0) = 0$, $p(r \to \infty, t) = 0$, $\partial p(r_w, t)/\partial r - \partial p/\partial t = F(t)$, *identical in form* to the dimensionless isotropic model. Thus, earlier results including $p_{exact}\ (r,t)$ apply. We now let $P_w(R_{eps},t)$ denote the dimensional pressure at the "ellipsoidal radius" R_{eps} describing the needle orifice. In transversely isotropic media, the prior isotropic "k" is replaced by $k_h^{2/3}k_v^{1/3}$. Early and late time solutions follow from

$$P(R_{eps},t)_{early\text{-}time} \approx P_0 - Q_0\, t/(VC) \quad (3a)$$

$$P(R_{eps},t)_{late\text{-}time} \approx P_0 - Q_0\, \mu/(4\pi R_w k_h^{2/3} k_v^{1/3}) + \{Q_0\, \mu/(4\pi k)\}\sqrt{\{(\phi\mu c/(\pi\, k_h^{2/3} k_v^{1/3} t)\}} \quad (3b)$$

As with isotropic problems, "early to intermediate time" expressions can be developed using standard series expansions; these will be discussed in inverse methods to follow. In Darcy analyses, a "mobility" is defined by k/μ in isotropic flow, representing net resistive effects due to the medium and the fluid. The Newtonian viscosity μ is assumed known from viscometer measurements. For transversely isotropic media, horizontal, vertical and effective mobilities are k_h/μ, k_v/μ and $k_h^{2/3}k_v^{1/3}/\mu$. "Forward solutions" for isotropic and transversely isotropic flows, since they follow from identical $p_{exact}\ (r,t)$ expressions, are combined in our **FT-00** algorithm utilizing the complete error function.

We emphasize that **FT-00** is exact and free of artificial viscosity and diffusion effects associated with numerical finite difference or element solutions. We later use **FT-00** to create exact "synthetic data" corresponding to prescribed input properties. To evaluate our approximate "inverse methods," arbitrary pairs of (time, pressure) points from synthetic pressure versus time curves are selected. These are used in inverse models to predict those tissue parameters assumed in creating the synthetic data. Both transient and steady inverse methods are summarized next.

Transient Transversely Isotropic Single Rate Inverse Solution for Liquids

Our exact pressure solutions can be used to derive inverse methods for tissue properties. Consider the early time solutions in Equations 1b or 3a. If discrete sets of early data were used to evaluate $P(R_w,t)$ and time t, and the results plotted with pressure on the vertical axis and time on the horizontal, the vertical intercept of the straight line gives the background pressure P_0. The slope of the straight line measured is $-Q_0/(VC)$. Since Q_0 and V are known, the value of C follows. In blood sampling, C represents a blood compressibility identical to c. For injection applications, C would characterize the injectate or a volume average of

it and any supplemental fluid in the flowline. This C also considers tubing flexibility when injectors are used. While P_0 is predicted as stated, it is error prone since initial tissue contacts may be erratic. A more precise method for P_0 is offered later.

Permeability prediction from "early to intermediate time" data is possible using the full error function solution in $P(r,t) = P_0 + p^* p(r,t)$ where p*, r and t are known. Here we assume constant rate pressure drawdown (continuous decreases in time) or buildup (increases) – these curves are simply reversed vertically in pressure versus time plots. We had noted how different series expansions for e^t and erfc(z) are available using exponentials and rational polynomials. In either case, the leading approximations in dimensional variables take the form $P_w(t) \approx P_0 + A\,H(Bt)$, where $P_w(t)$ is the unsteady needle orifice pressure, H(B) is a known function of B depending on the expansion used, and $A = \mu Q_0/(4\pi R_w k_h^{2/3} k_v^{1/3})$ and $B = 4\pi R_w k_h^{2/3} k_v^{1/3}/(\mu VC)$ are positive.

For inverse applications, suppose that $P_w(t)$ is available at three times, that is, $P_{w,\#1}$ at t_1, $P_{w,\#2}$ at t_2 and $P_{w,\#3}$ at t_3, with # emphasizing measured data. The unknown parameters to be determined are P_0, the effective mobility $k_h^{2/3} k_v^{1/3}/\mu$ and the compressibility C. The latter two quantities are deducible from A and B, whose values are numerically first obtained. Initially we write our data relations as $P_{w,\#1} - P_0 \approx A\,H(Bt_1)$, $P_{w\#2} - P_0 \approx A\,H(Bt_2)$ and $P_{w,\#3} - P_0 \approx A\,H(Bt_3)$, where the left sides are measured changes relative to background pressure. Next we divide the first equation by the second, showing that $H(Bt_1)/H(Bt_2) \approx (P_{w,\#1} - P_0)/(P_{w,\#2} - P_0)$ where the right side is known from empirical or synthetic data.

The above equation, independent of A and P_0 and containing only the unknown B, represents a nonlinear equation for B expressed in terms of H. Since $H(Bt_1)/H(Bt_2)$ is a monotonic function of B, trial B values can be determined iteratively by incrementing from zero until the right-side quantity is achieved. A half-step corrective procedure can be used to accelerate convergence. Once B is known, the first equation $P_{w,\#1} - P_0 \approx A\,H(Bt_1)$ can be used to determine A since "$P_{w,\#1} - P_0$" is known. With A and B available, the third equation can be used to predict P_0 where t_3 information is used. As noted, $k_h^{2/3} k_v^{1/3}/\mu$ and the compressibility C are calculated from A and B. Thus, $k_h^{2/3} k_v^{1/3}/\mu$, C and P_0 are fully determined. To obtain the tissue porosity φ, we derive Equation 3c from our late time formula; then, φ is obtained by substituting the necessary parameters and any $P(R_w,t)$ measurement in software.

Module POROSITY

$$\varphi = \{16\pi^3 k_{eff}^{\ 3} t/(Q_0^{\ 2}\mu^3 c)\}\{P(R_{eps},t) - P_0 + (Q_0\mu)/(4\pi R_w k_{eff})\}^2 \quad (3c)$$

The permeability method, requiring three time and pressure data pairs, utilizes data from the first seconds of measured syringe transients. If the time from needle contact to pressure equilibrium is fifteen seconds, data from 0, 7 and 15 sec would ensure linear independence of the equations used. When steady conditions are so rapidly achieved that separated data points are difficult to obtain, the time window Δt for data acquisition must be widened. Analysis shows that Δt increases with the product VC, and importantly, that predicted permeabilities are independent of VC. A long liquid filled tube (to increase V) separating syringe body from pump will expand Δt. Alternatively, the syringe body can host supplemental gas of high compressibility C, separated by a movable flexible membrane from the injectate. This simple modification enhances syringe portability. When VC altering fixes are used, predicted compressibilities are no longer that for the tissue, but predictions for $k_h^{2/3} k_v^{1/3}/\mu$, k_h/μ, k_v/μ and P_0 importantly remain unaffected. While we have described inverse solutions for single rate applications, that is, for pressures arising from continuous withdrawal or injection, dual rate approaches can be similarly treated using an analogous H function modified by superposition methods previously described. Single and dual rate models are solved by software **Modules PTA-APP-01B** and **FT-PTA-DDBU**.

Inverse Solutions for k_h and k_v from Steady Pressure Drop Data for Liquids

The foregoing inverse method assumes transient pressures available at the needle tip or at close locations within the syringe housing. For such single-transducer syringes, only the effective permeability $k_h^{2/3} k_v^{1/3}$ is predictable. Here we consider dual-transducer designs where pressure data from an additional sensor are available at an external needle surface location in contact with the tissue. We assume that the angle δ between syringe and vertical permeability axes is known, as is the distance L between external and tip sensors (see Figure 2). If ΔP_d and ΔP_s represent steady pressure drops measured at equilibrium, and Q_0 and R_{eps} are constant rate and ellipsoidal radius, asymptotic analysis shows that k_h, k_v and k_h/k_v satisfy

$$\cos^2\delta\, k_h^{\ 3} - Q_0^{\ 2}\mu^2/(16\pi^2\Delta P_d^{\ 2} L^2)\, k_h - Q_0^{\ 3}\mu^3 \sin^2\delta/(64\pi^3 R_{eps}^{\ 3}\Delta P_s^{\ 3}) = 0 \quad (4a)$$

$$\{Q_0^{\ 3}\mu^3 \sin^2\delta/[64\pi^3 R_{eps}^{\ 3}(P_0 - P_s)^3]\}\, k_v^{3/2} - \{Q_0^{7/2}\mu^{7/2}/[128\pi^{7/2} L^2 R_{eps}^{\ 3/2}(P_d - P_0)^2 (P_0 - P_s)^{3/2}]\}\, k_v + \{\mu^{9/2} Q_0^{9/2}\cos^2\delta/[512\pi^{9/2} R_{eps}^{\ 9/2}(P_0 - P_s)^{9/2}]\} = 0 \quad (4b)$$

$$\{\cos^2\delta\,\mu^3 Q_0^{\ 3}/[64\pi^3 R_{eps}^{\ 3}(P_0 - P_s)^3]\}(k_h/k_v) - \{Q_0^{\ 3}\mu^3/[64\pi^3 L^2 R_{eps}(P_d - P_0)^2 (P_0 - P_s)]\}(k_h/k_v)^{1/3} - \{Q_0^{\ 3}\mu^3 \sin^2\delta/[64\pi^3 R_{eps}^{\ 3}(P_s - P_0)^3]\} = 0 \quad (4c)$$

In drug delivery and artificial organ design applications, k_h and k_v values may be individually required. They can be obtained from cubic Equations 4a-4b. These do not contain

compressibility effects since they disappear at large times. To determine C or c, complementary single-sensor, early-time transient inverse procedures are required. Software **Module FT-01** solves Equations 4a,b,c.

Syringe Hardware Modifications

Different single syringe designs are available as shown in Figure 3. Essentially, a needle contacts tissue at **5**, located near internal pressure sensor **1**. Measured pressures p_{exact} (r_w,t) are extremely close to those at **2** and **3**, also immersed in the syringe fluid. These contrast with external transducers **4A** and **4B** in direct tissue contact measuring p_{exact} $(r > r_w, t)$. For designs with internal sensors only, transient inverse methods will yield c or C, $k_h^{2/3}k_v^{1/3}$, P_0 and φ. When an additional external transducer is used, steady-state tests will give k_h and k_v individually, but not compressibility, pressure and porosity.

In applications where pressures equilibrate so rapidly that accurate multi-point (time, pressure) data acquisition is not possible, time window widths can be amplified by increasing the value of VC. This is accomplished by introducing a long flexible liquid filled tube **18** between syringe fluid and auto-injector or infusion pump. If portability is essential, one may instead introduce a movable flexible membrane within the syringe, separating the near fluid **8** and a compressible gas **12**. The use of non-toxic filtered room air drawn through a one-way check valve provides a simple solution. Flush mounted pressure transducers and embedded wiring are assumed, whose electrical signals are digitized and processed in computer control unit **10**.

Single needle diagnosis may be limiting when properties over a broader region are required. Multi-needle syringe arrays can be used. The top left of Figure 4 shows easily inserted parallel needles with adjustable depth. The right diagram shows multiple needles operating at different inclinations and depths. Markings at syringe tops allow needle source and observation positions within tissues to be determined from direct calculation for use in forward and inverse simulators. Sketch D shows how source points A and B might define a "virtual needle" of known inclination. Note that numerous combinations of pressure data taken from multiple needles provide properties for detailed heterogeneity and anisotropy mapping. Finally, the bottom left of Figure 4 shows an internal "red hook" or biopsy sampler that removes tissue samples upon syringe withdrawal. Such sampling can be used together with pressure transient analysis.

Results for Several Challenging Imaging Problems

Subcutaneous Injection and Permeability in Humans

Needle-free injection methods using high speed fluid jets, together with strong pressure interactions within "intelligent" syringe housings, have been studied in recent years. However, our use of "intelligent syringes" and general Darcy pressure transient analyses for tissue properties is completely new. Literature searches uncovered two pharmaceutical investigations where transient profiles were measured, providing important data to evaluate our ideas. Both focused on pain threshold dependence on injectate volume, viscosity and flow rate. These were interested more in steady "plateau pressures" (as in Figure 1) than the unsteady pressures underlying our research. Math validations showing consistency between forward and inverse models are reported later. Here we discuss clinical applications demonstrating the versatility of *i* Syringe analysis.

"Clinical evaluation of large volume subcutaneous injection tissue effects, pain, and acceptability in healthy adults," provides detailed pressure transients duplicated in

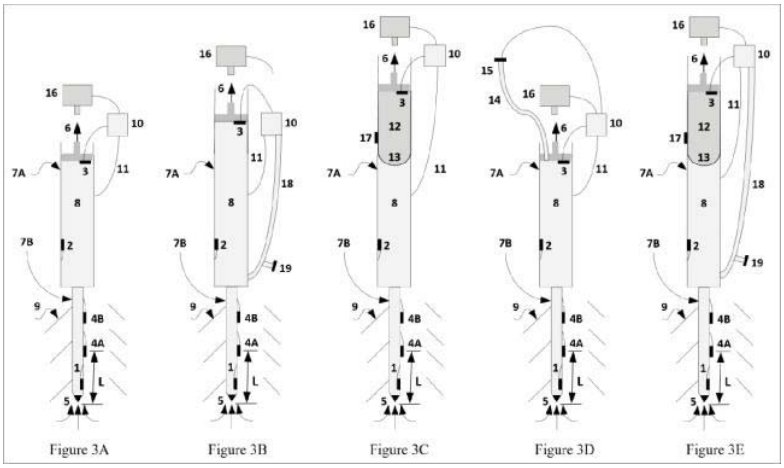

Figure 3. Single-needle syringes, with flush mounted "internal pressure transducers" **1**, **2** and **3**, and "external transducers" **4A** and **4B**. Items **6**, **16** and **10** represent plunger, speed control and computer. Movable flexible membrane **13** separates injectate **8** and supplemental fluid **12** (pressures are continuous across membrane). Cross-hatching denotes tissue media.

Wilson C. Chin et al., Int J Appl Biol Pharm 2024
DOI:10.26502/ijabpt.202132

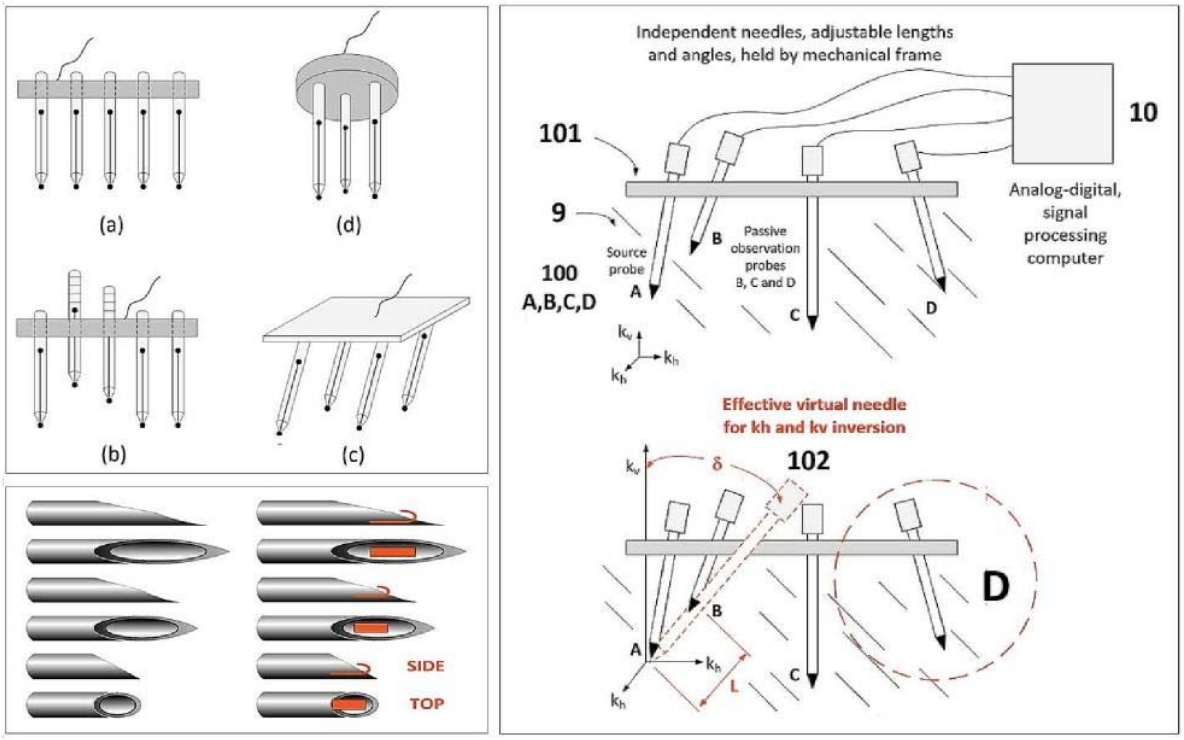

Figure 4. Multi-needle syringes, parallel needle arrangement (top left); adjustable retractable lengths and angles with contoured flexible base (right). Beveled tip with "biopsy sampler" (bottom left).

Figure 5-*I* [2]. Traces A, B and C deal with 5 ml injections for 1.1, 8 and 20 cp viscosities, while Trace D presents results for 10 ml and 20 cp. The paper notes that "each curve is the mean value of all included injections." These smoothed results therefore cover "thirty-two adult male and female subjects ranging from 18-65 years of age, where a total of 192 injections were administered." Thus, our conclusions below apply to an "averaged human" and not to any individual. Also, the higher viscosity fluid was non-Newtonian, with stress data obtained at two unspecified shear rates. This differs from the Newtonian model in our Darcy equations. Finally, the authors did not comment on compressibility and anisotropy, while frictional flowline effects were unaccounted for. Our predictions should be understood in light of these limitations.

Exercise 1. Here we will consider Trace D in Display *I*. We study the left side *buildup* using inverse **Module PTA-APP-01B**. The data used are #1 (t = 0 sec, P = 0 psi), #2 (t = 2.5 min = 150 sec, P = 53 psi) and #3 (t = 8 min = 480 sec, P = 60 psi). The needle radius was not given – we assumed a 0.01 cm radius. The flow rate for Traces A, B, C and D is –0.02 cc/s. Calculations yield a k_{eff} of 39.36 md/cp. Predicted compressibility is large at 0.00029/psi and includes long flexible tubing effects. Alternatively, we can use *drawdown* data with model **FT-PTA-DDBU**. Points selected visually are #1 (t = 8 min = 480 sec, P = 60 psi), #2 (t = 10 min = 600 sec, P = 18 psi) and #3 (t = 18 min = 1,080 sec, P = 7 psi). Results in Figure 5, Display *II* bottom right give a mobility of 44.45 md/cp, comparing favorably with 39.36 md/cp. The 7 psi pressure may be inaccurate, but not surprising given the experimental inconsistencies cited.

Compressibility and flowline volume influence is interesting, with Woodley's experimental setup suggesting strong fluid cushioning effects. As details are not available, we assumed in **PTA-APP-01B** a value of 80 cc as in related work [3] considered separately. Substitution in `Compressibility (1/psi): 0.2330E-01 x (cc/FloLineVol)` leads to a 0.00029/psi compressibility (versus 0.00061/ psi in the related investigation). In both studies, flowlines were constructed from long flexible tubes which enhanced "VC" compressibility. Large values of VC widen time measurement windows, rendering pressure signals visible and easily measurable. As a check, we used **FT-00** to create an implied pressure waveform. When times from Figure 5, Display *I* are expressed in seconds, and a compressibility of 0.00029/psi is used, together with permeability taken as (predicted mobility, 40 md/cp) × (input viscosity, 20 cp) or 800 md, the line obtained in Figure 5, Display *III* agrees with Trace D. Thus the results of **Modules PTA-APP-01B**, **FT-PTA-DDBU** and **FT-00** are consistent.

Wilson C. Chin et al., Int J Appl Biol Pharm 2024
DOI:10.26502/ijabpt.202132

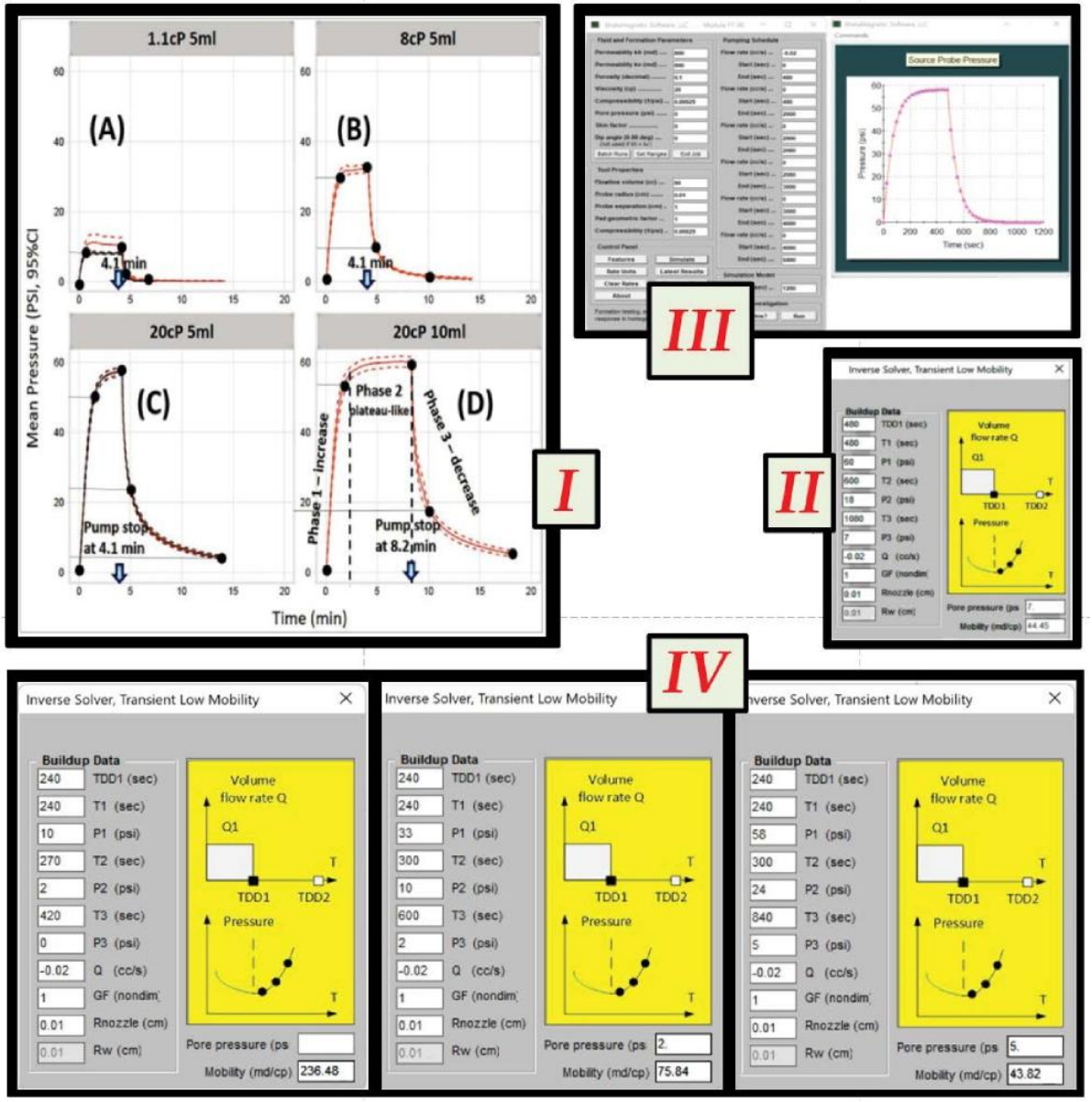

Figure 5. Display I from Woodley et al. (2022), red denoting abdomen and black the thigh [2]. Data circles and A, B, C and D labels are ours. Blue arrows denote time when pumping stopped. Authors noted "initial rise, plateau region and decline after injection ceases" as discussed in our Figure 1.

Exercise 2. Here we will demonstrate the use of inverse methods in trend analysis by studying pressure decline in Traces A, B, C (buildup traces were excluded due to an unrealistic plateau at the top of Trace A). Thus, we apply **Module FT-PTA-DDBU**. For A, we use #1 (t = 4 min = 240 sec, P = 10 psi), #2 (t = 4.5 min = 270 sec, P = 2 psi) and #3 (t = 7 min = 420 sec, P = 0 psi). For B, we use #1 (t = 4 min = 240 sec, P = 33 psi), #2 (t = 5 min = 300 sec, P = 10 psi) and #3 (t = 10 min = 600 sec, P = 2 psi). And for C, we use #1 (t = 4 min = 240 sec, P = 58 psi), #2 (t = 5 min = 300 sec, P = 24 psi) and #3 (t = 14 min = 840 sec, P = 0 psi). We assumed a Needle Gauge 27 syringe with an inner radius of 0.01 cm since needle size data was not available, and further, that all 5 ml flow rate tests were performed with the same syringe.

Figure 5-IV 's predicted spherical mobilities for A, B and C, namely 236, 76 and 44 md/cp for viscosities 1.1, 8 and 20 cp, are interesting. They differ enough that our visual selection of pressure input data should not introduce sizable error. Similarly, viscosity values are well separated. From "Permeability = Mobility × Viscosity," we have, going from A to C, the permeabilities (236)(1.1) or 260, (76)(8) or 608

and (44)(20) or 880 md, respectively. For the data analyzed, the permeabilities are increasing as pressure increases.

The predictive methods disclosed in this paper were derived from geosciences algorithms popular in oil and gas exploration developed by the first author. These have been used for almost three decades and are treated in several books from John Wiley & Sons and Elsevier Scientific Publishing (see "Discussion and Closing Remarks").

In geological engineering, decreases in rock and soil permeability are found as pressure increases. These arise from mechanical compaction and imply increased flow resistance as interstitial spaces reduce in size. Often, however, as in "hydraulic fracturing," very high stress loadings introduce high permeability microfractures that allow increased oil production and the opposite occurs. In biomedical applications, complicated permeability changes are affected by capillary, cellular and other microscopic phenomena. Our methods, which only measure increases or reductions, do not explain them.

Investigators have speculated that high pressure damage at injection zones may lead to inflammation and permeability increases as flow increases from capillaries to surrounding tissues. Permeability issues of significance to *i*Syringe applications are discussed in recent studies [4,5,6,7]. For example, the latter explores "elevated capillary permeability," "increases in hydraulic conductivity" and "increased tissue permeability" using finite element solutions to lower limb swelling. Recent works on cancer and tumor growth importantly show how sustained permeability increases encourage rapid growth by increasing nutrients and oxygen delivery. In our literature searches, we have not uncovered direct permeability data for human tissues – results inferred from interpreted pressure responses, such as ours, offer clues to this important property.

Yorkshire Swine Fluid Mobility and Needle Size Effects

"Understanding Subcutaneous Tissue Pressure for Engineering Injection Devices for Large-Volume Protein Delivery" provides waveforms useful to extracting properties from dynamic pressure data [3]. It summarizes results for "self-administration of monoclonal antibodies using prefilled syringes, autoinjectors, and on-body injector devices," investigating subcutaneous pressures and injection site reactions as functions of injection volume, flow rate and viscosity and formulation. Since back pressure is an indicator for changes in mechanical tissue properties leading to pain, buildup and decay times as well as pain thresholds were monitored. Swine porcine models were selected to simulate human subcutaneous injections given similarities in tissue thickness. A pressure sensor in the fluid path recorded subcutaneous pressures in the abdomen of Yorkshire swine.

The setup used, emphasizing long tubular connections totaling forty inches, is duplicated in Figure 6. Pressure drops in the main line were subtracted from total pressures, using data obtained from air measurements (we address total compressibility later). Here we are interested only in pressure transients. Since p_{exact} (r_w,t) is smooth, outliers A and C were discarded in favor of Trace B. This describes realistic subcutaneous reactions, with a 20 sec buildup time providing sufficient time for measurement.

Orifice sizes were not specified so we take this opportunity to consider those mobilities predicted if Trace B data had been collected with needles of different radii. Pressure data #1 (t = 0 sec, P = 0 psi), #2 (t = 6 sec, P = 5.8 psi) and #3 (t = 19 sec, P = 7 psi) were used in inverse **Module PTA-APP-01B** with a flow rate of – 0.1 cc/s. For Runs *I*, *II* and *III*, we assume inner needle radii of 0.01 cm, 0.05 cm and 0.10 cm to calculate mobility. We find that *I* predicts a 1,681 md/ cp, while *II* yields a smaller 336.2 md/cp, with *III* leading to a further reduction with 168.1 md/cp. For example, 1,000 md/ cp may represent the permeability of ordinary sand to water, while values less than 0.1 md/cp describe much denser rocks.

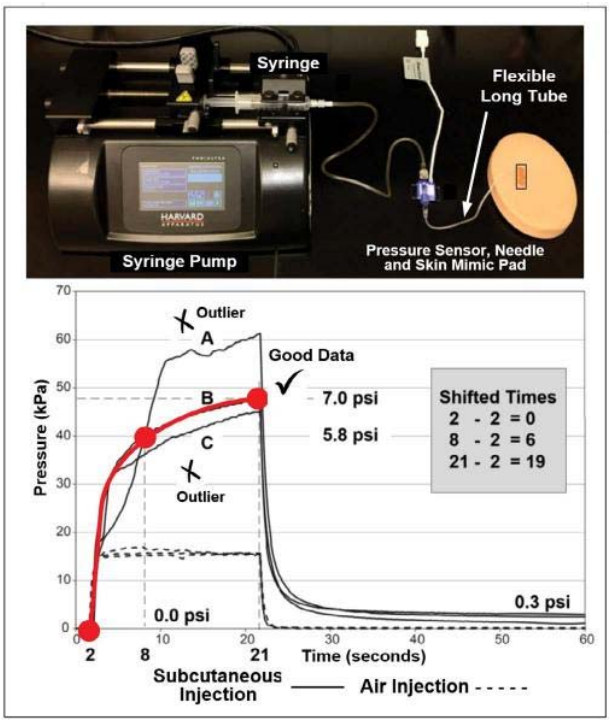

Figure 6: Yorkshire swine test fixture (Doughty et al. (2016) or [3], our annotations).

Forward and Inverse Model Validations

How do we assess the quality of predicted tissue properties? Experimental approaches are not entirely reliable, since test samples cannot be accurately characterized. In our approach, exact pressure versus time solutions corresponding to a

well accepted forward Darcy formulation provide synthetic "patient" test data with which to evaluate approximate inverse models. If predicted permeabilities, compressibilities and pressures agree with values used in creating our synthetic data, one would conclude that both forward and inverse models are consistent and accurate. Here we present method validations focusing on applications and input numbers encountered in practice.

Example 1. Results for Isotropic Media Using Drawdown Method.

The input menu in Figure 7 assumes an isotropic permeability of 1 md, a viscosity of 1 cp, for a mobility of 1 md/cp. A compressibility of 0.000003/psi (approximately that of water) is used with a tissue porosity of 0.15. The syringe dip angle is vertical at zero degrees. The needle radius is taken as 0.05 cm. We assume a 1 cm separation distance for an optional second observation transducer in direct tissue contact. The flow rate as taken as 0.01 cc/sec for five seconds while the syringe flowline volume is 5 cc. The high 1,000 psi background hydrostatic pressure, not dynamically significant, was chosen so displayed pressures are positive. Calculated and plotted pressures appear in Figure 7.

We perform an inverse calculation using the early-time method in **PTA-APP-01B**. We have selected pressure data at 0.0, 0.3 and 0.6 sec. Computer output is shown in `Courier font`.

```
OUTPUT SUMMARY ...

Volume flow rate Q1 (cc/s): 0.100E-01
   Pump probe, radius (cm): 0.500E-01
   Probe, geometric factor: 0.100E+01
     Effective radius (cm): 0.500E-01
   1st Point Time T1 (sec): 0.000E+00
         Pressure P1 (psi): 0.100E+04
   2nd Point Time T2 (sec): 0.300E+00
         Pressure P2 (psi): 0.866E+03
   3rd Point Time T3 (sec): 0.600E+00
         Pressure P3 (psi): 0.810E+03

Pore pressure and mobility predicted ..
          Pore pressure (psi) : 0.1000E+04
   Spherical mobility (md/cp): 0.1018E+01

   FloLineVol*Comp (cm^5/lbf) : 0.9709E-04
      Compressibility (1/psi) : 0.1505E-04
                    x(cc/FloLineVol)
```

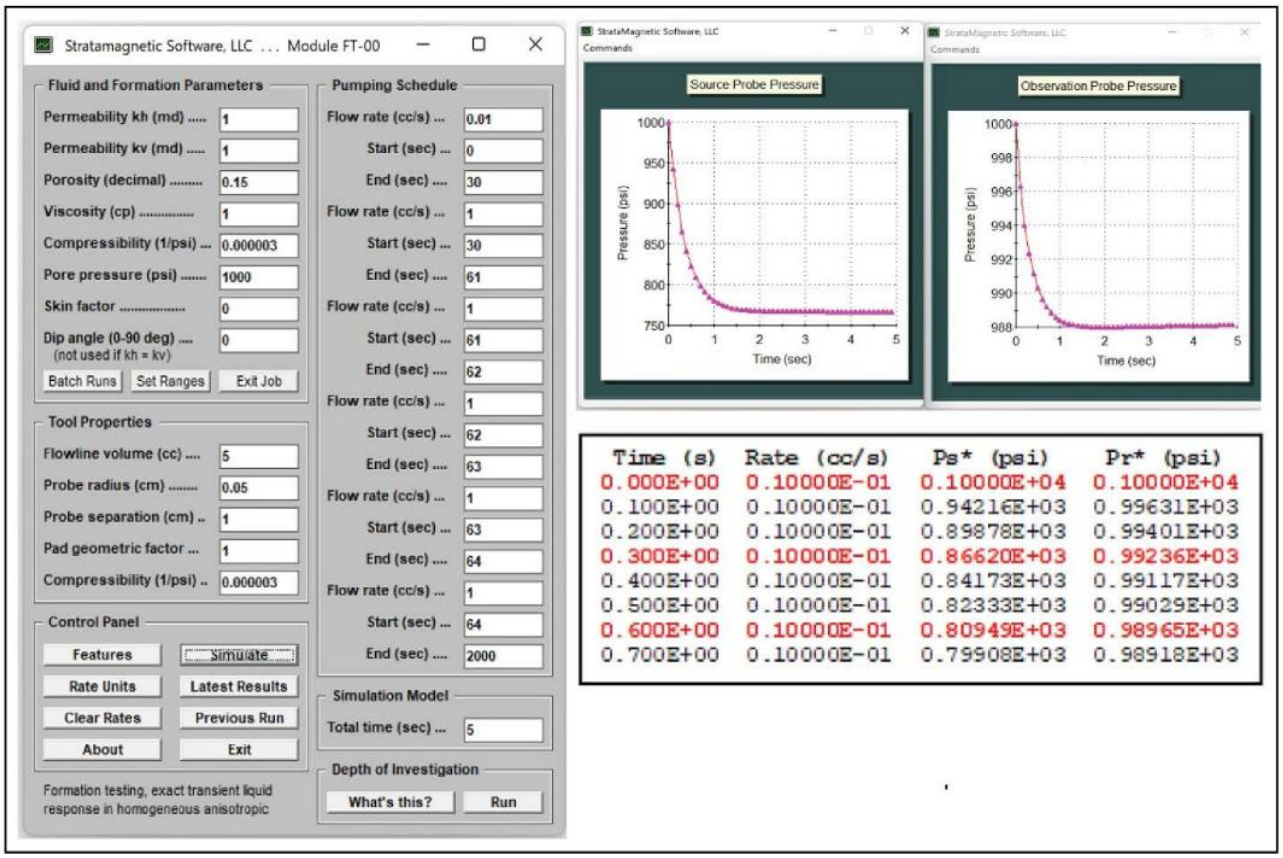

Time (s)	Rate (cc/s)	Ps* (psi)	Pr* (psi)
0.000E+00	0.10000E-01	0.10000E+04	0.10000E+04
0.100E+00	0.10000E-01	0.94216E+03	0.99631E+03
0.200E+00	0.10000E-01	0.89878E+03	0.99401E+03
0.300E+00	0.10000E-01	0.86620E+03	0.99236E+03
0.400E+00	0.10000E-01	0.84173E+03	0.99117E+03
0.500E+00	0.10000E-01	0.82333E+03	0.99029E+03
0.600E+00	0.10000E-01	0.80949E+03	0.98965E+03
0.700E+00	0.10000E-01	0.79908E+03	0.98918E+03

Figure 7. **FT-00** and **PTA-APP-01B** isotropic drawdown calculations.

Wilson C. Chin et al., Int J Appl Biol Pharm 2024
DOI:10.26502/ijabpt.202132

These results are very satisfactory. The background pressure is recovered as 1,000 psi while a mobility of 1.018 md/cp is predicted with less than 2% error. The compressibility output "0.1505E-04 x (cc/FloLineVol)," using the 5 cc substitution, yields a value of 0.00001505/5 1/psi or 0.00000301/psi (compared to an input of 0.000003/ psi). Next we calculate porosity from **Module POROSITY**. With an isotropic permeability of 1 md, a viscosity of 1 cp, a flow rate of 0.01 cc/sec, a needle radius of 0.05 cm, a compressibility of 0.000003/psi and a background pressure of 1,000 psi, the porosity values for time-pressure data at 2, 3, 4 and 4.9 sec are

```
Time(sec 2.,P(psi) 768.1, POR 1.79
Time(sec 3.,P(psi) 767.2, POR 0.26
Time(sec 4.,P(psi) 767.1, POR 0.20
```

```
Time(sec) = 5., P(psi) = 767.1, POR = 0.24
```

compared with an exact **FT-00** input of 0.15. In general, porosity results are less reliable than those for permeability, compressibility and pressure, since the parameter inputs used are themselves approximate predictions. In practice, porosity numbers should be used judiciously.

Example 2. Results for Transversely Isotropic Media for Pure Drawdown or Buildup.

Many body tissues exhibit transversely isotropic behavior. In this first run, at the top of Figure 8, we revisit Example 1 but assume k_h = 1 md and k_v = 5 md. We perform the drawdown shown and carry the simulation to steady-state. Again forward Module **FT-00** provides exact synthetic pressure data for steady inverse method **FT-01**, also exact. Calculated transient pressures appear in Figure 8 and in the listing following it.

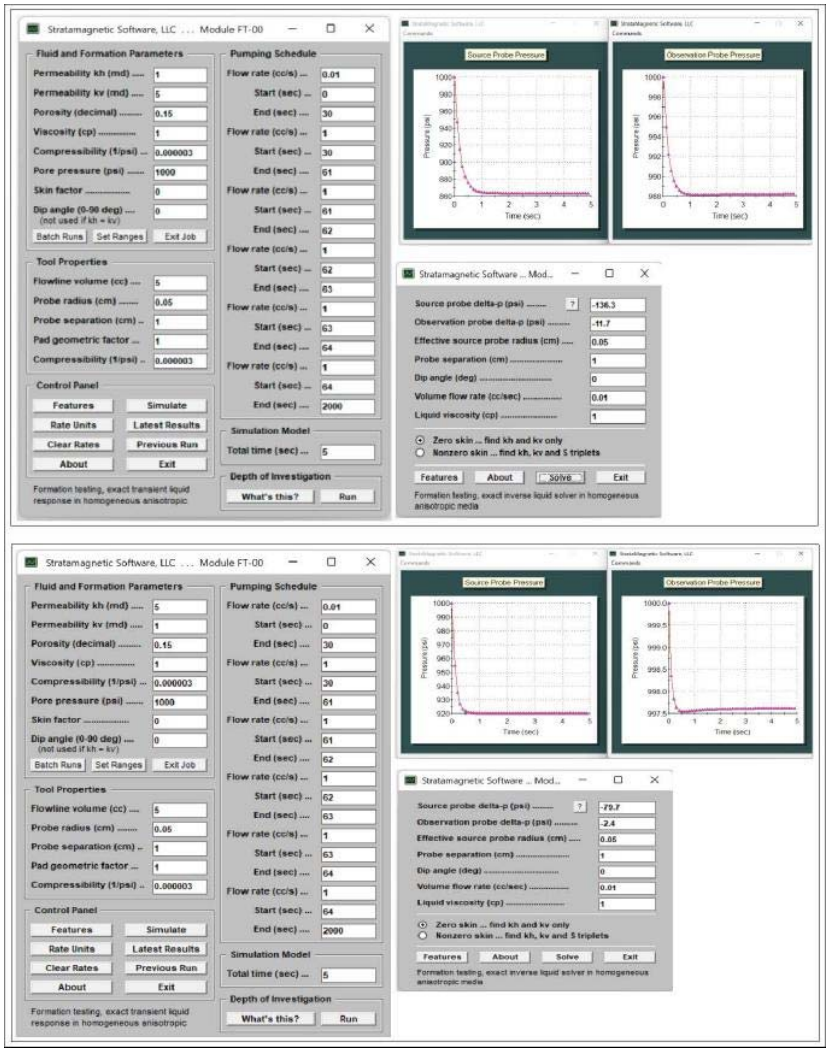

Figure 8. **FT-00** and **FT-01** transversely isotropic calculations.

```
  Time (s)    Rate (cc/s) Ps* (psi) Pr*(psi)
0.000E+00  0.10000E-01 0.10000E+04  0.10000E+04
0.100E+00  0.10000E-01 0.94743E+03  0.99500E+03
0.200E+00  0.10000E-01 0.91524E+03  0.99223E+03
0.300E+00  0.10000E-01 0.89550E+03  0.99057E+03
0.400E+00  0.10000E-01 0.88337E+03  0.98959E+03
0.500E+00  0.10000E-01 0.87591E+03  0.98899E+03
0.100E+01  0.10000E-01 0.86497E+03  0.98820E+03
0.200E+01  0.10000E-01 0.86382E+03  0.98819E+03
0.300E+01  0.10000E-01 0.86377E+03  0.98822E+03
0.490E+01  0.10000E-01 0.86373E+03  0.98825E+03
```

We now perform inverse calculations using steady flow **Module FT-01**, also exact. Errors only arise when the pressure drops used have not fully equilibrated. From t = 4.9 sec results, the pressure drop at the source probe is 1000 - 863.7 or 136.3 psi while that at the observation probe is 1000 - 988.3 or 11.7 psi. The algorithm solves cubic equations and three roots are obtained,

```
Tentative permeabilities (md) ...

Complex KH root # 1: -.997E+00 + 0.000E+00 i,
KV: 0.504E+01

Complex KH root # 2: 0.997E+00 + 0.000E+00 i,
KV: 0.504E+01

Complex KH root # 3: -.196E-05 + 0.000E+00 i,
KV: 0.130E+13
```

Note that Roots 1 and 3 possess negative k_h values and Root 3 solutions are physically unreasonable. On the other hand, Root 2 successfully predicts k_h = 0.997 md and k_v = 5.04 md, which are close to the **FT-00** inputs of k_h = 1 md and k_v = 5 md.

In a second simulation for this Example 2, consider the nontrivial case with reversed k_h = 5 md and k_v = 1 md inputs relative to the first, as shown at the bottom of Figure 8. Computed forward **FT-00** results are given there and also immediately below.

```
Time (s) Rate (cc/s) Ps* (psi) Pr* (psi)
0.000E+00  0.10000E-01 0.10000E+04  0.10000E+04
0.100E+00  0.10000E-01 0.95498E+03  0.99836E+03
0.200E+00  0.10000E-01 0.93548E+03  0.99783E+03
0.300E+00  0.10000E-01 0.92700E+03  0.99763E+03
0.400E+00  0.10000E-01 0.92330E+03  0.99756E+03
0.500E+00  0.10000E-01 0.92168E+03  0.99754E+03
0.100E+01  0.10000E-01 0.92039E+03  0.99757E+03
0.400E+01  0.10000E-01 0.92030E+03  0.99762E+03
0.490E+01  0.10000E-01 0.92029E+03  0.99763E+03
```

The inverse calculation is initiated at the bottom of Figure 8. For the required steady pressure inputs, we use values at t = 4.9 sec, for which pressure drops are found as 1000 – 920.3 or 79.7 psi and 1000 – 997.6 or 2.4 psi at source and observation probes. Calculated results are displayed below. As before, Roots 1 and 3 are associated with physically invalid solutions. On the other hand, the result in Root 2 is very good, with k_h = 4.86 md and k_v = 1.06 md as compared to **FT-00** inputs of k_h = 5 md and k_v = 1 md.

```
Tentative permeabilities (md) ...

Complex KH root # 1: -.486E+01 + 0.000E+00 i, KV:
0.106E+01

Complex KH root # 2: 0.486E+01 + 0.000E+00 i, KV:
0.106E+01

Complex KH root # 3: -.956E-05 + 0.000E+00 i, KV:
0.274E+12
```

Example 3. Results for Transversely Isotropic Media Using Drawdown-Buildup Method.

Now consider transversely isotropic media with a drawdown-buildup sequence. Synthetic data is created using **FT-00** for input into the inverse drawdown-buildup **FT-PTA-DDBU** model, which predicts background pressure and $k_h^{2/3}$ $k_v^{1/3}$. We will show that predictions are consistent with the inputs used to create the synthetic data in the forward model. While "transversely isotropic" appears in the title, the method also applies to purely isotropic media.

Calculated source pressure versus time together with assumptions appear in Figure 9 (next page). The initial syringe drawdown terminates at t = 3 sec, at which point pressure increases. The inverse menu for **FT-PTA-DDBU** shows arbitrarily selected pressures from t = 3, 4 and 5 sec which have not yet equilibrated in time. At the bottom-right of the inverse code menu, the predicted steady background pressure at large times is 1,001 psi, which is close to the 1,000 psi assumed. In addition, the spherical mobility is predicted as 0.3 md/cp, which very close to that assumed in the forward simulation, that is, $(0.5)^{2/3}$ $(0.1)^{1/3}$ or 0.2924 md/cp. Thus, the exact **FT-00** model and approximate **FT-PTA-DDBU** superposition inverse method for drawdown-buildup sequences are numerically consistent.

Effects of Compressibility

Compressibility appears as "c" in the differential equation, referring to the tissue medium, and "C" in the syringe constraint describing fluid in both syringe and flowline. At steady-state, all $\partial P/\partial t$ terms vanish and neither φc nor VC affects the dynamics – only true mobility effects like "k_{eff}/μ" remain. Figure 10 shows pressure calculations performed for two very different compressibilities. Note how the character of the computed line curves differ.

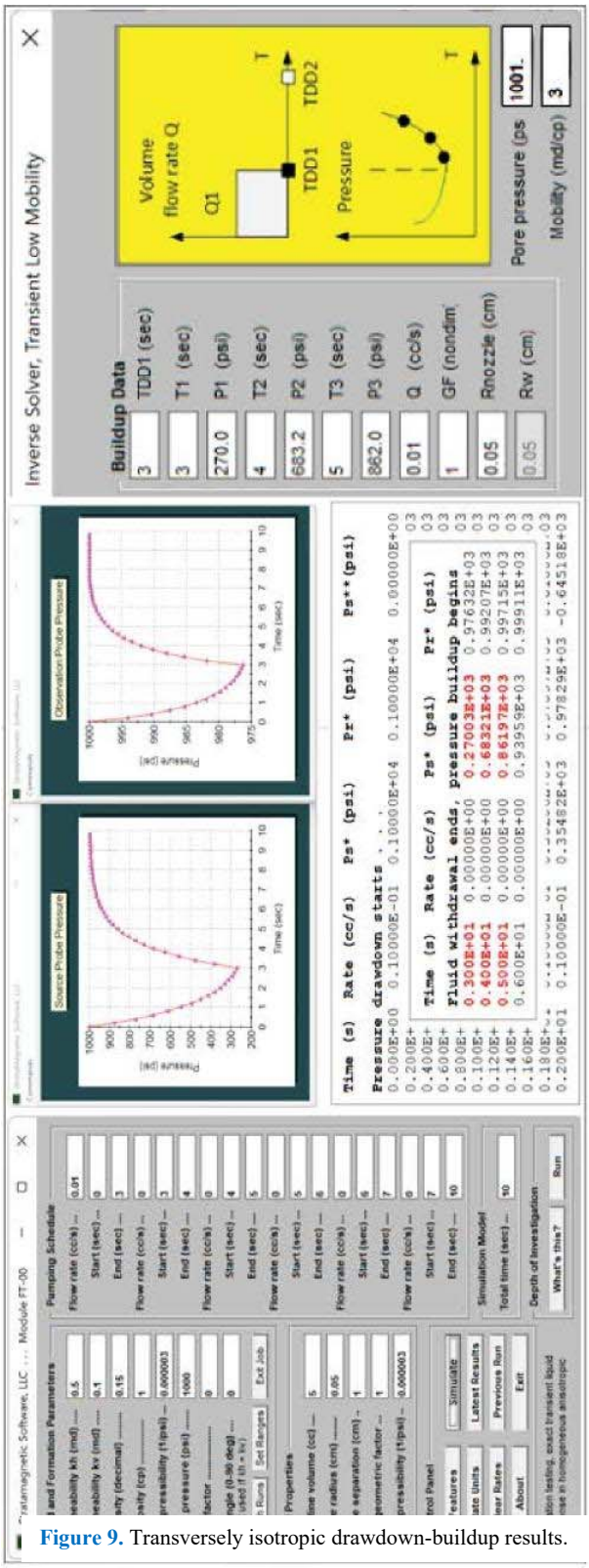

Figure 9. Transversely isotropic drawdown-buildup results.

Pressure histories are created in Figure 10 for our "1,681 md Yorkshire swine problem" using **FT-00**. The upper curve assumes the **FT-01** predicted compressibility of 0.00061/psi while the lower diagram assumes a much smaller water 0.000003/psi consistent with the injectate in the experiments. All input parameters are otherwise identical. The top curve reproduces the experimentally observed pressure curve in Figure 6. Note how both pressure traces yield the same 7 psi steady pressure drop despite large compressibility differences. This depends *only* on the mobility in the medium. Importantly, the upper curve smoothly equilibrates in 20 sec; the lower curve achieves steady state in one second, seen in the steep, barely visible line near t = 0.

Thus, higher VC values broaden the time window available for data acquisition, allowing greater accuracy while leaving predicted permeability or mobility unaffected. If steady states are achieved too rapidly, simply install a long liquid filled flexible tube between needle and syringe pump. Alternatively, introduce a movable flexible membrane **13** as shown in Figure 3, separating the injectate **8** and a supplemental compressible gas **12** such as air. Long liquid filled tubing works well, but the use of compressible gases is suggested for syringe portability.

Subtle Flowline Geometry and Frictional Considerations

Subtle effects related to flowline geometry and friction on permeability prediction are offered based on **FT-00** and **PTA-APP-01B** calculations. Using $k_h = 30$ and $k_v = 20$ md, we have $k_{eff} = (30)^{2/3}(20)^{1/3} = 26.21$ md. To emphasize key ideas, we use extreme values for certain parameters. In Run 1, we assume a typical V = 10 cc and a 0.02 cc/s injection rate. Transient pressures equilibrate within 0.5 sec to 90 psi. Calculated pressure values at 0.0, 0.2 and 0.4 sec are used in **PTA-APP-01B**. The predicted k_{eff} is 26.56 md/cp, implying a 26.56 md permeability for the 1 cp fluid, a small 1% error. This validates forward and inverse methods, but in practice, the 0.5 sec time window is too small to ensure measurement accuracy given initially erratic needle movements. In Run 2, we consider the effects of large flowline volumes and friction.

For Run 2, we consider extended syringe and flowline volume effects. Longer line extensions are a necessity in laboratory work with pressure sensors placed at the distant end away from the needle [2,3]. One might suppose that sensors closest to the orifice would provide greater accuracy in properties prediction. After all, transducers located faraway experience wall friction pressure drops arising from fluid movement. The added volume would also increase cushioning effects due to compressibility. How do these effects influence permeability prediction? We first run **FT-00** for a long 10,000 cc flowline compared to 10 cc. The pressure solution equilibrates to the same 90

Wilson C. Chin et al., Int J Appl Biol Pharm 2024
DOI:10.26502/ijabpt.202132

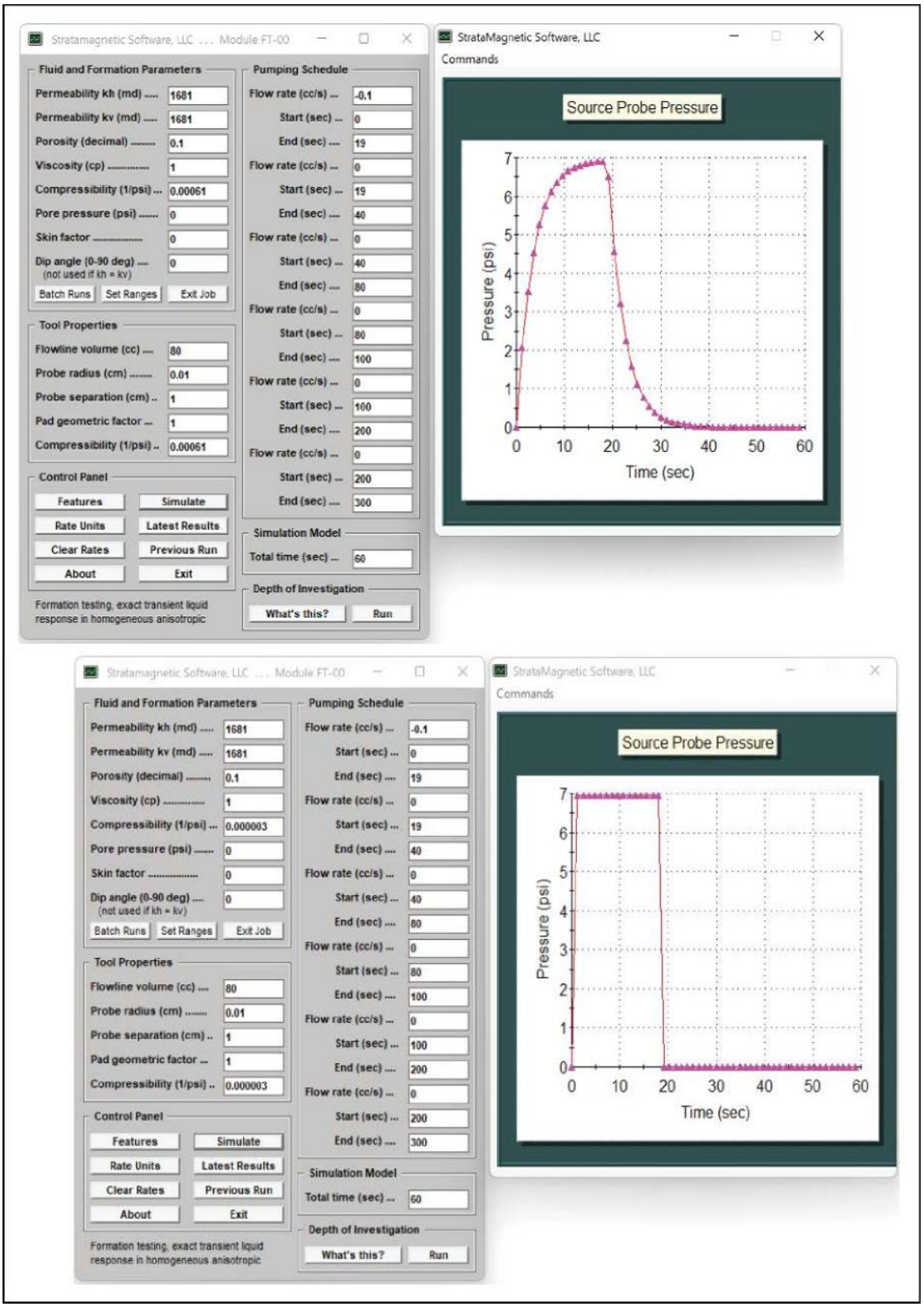

Figure 10. **FT-00** pressure plots for "Yorkshire swine problem" using C = 0.00061/psi (upper) and C = 0.000003/psi (lower).

psi, not surprising since VC and φμc terms disappear at large times. But what is interesting is the broader time window available for measurement. The dynamically significant time interval extends to about 300 sec from 0.5 sec, providing greater flexibility for measurement accuracy. Are predicted permeabilities affected? **PTA-APP-01B** results again show a k_{eff} of 26.56 md as in Run 1. This result is welcome. We conclude that the added compressibility associated with longer flowlines is desirable because larger time windows available for data acquisition are encouraged.

We have not discussed the effects of constant rate fluid movement in the flowline. Assume a viscosity such that the end transducer measures an additional 1,000 psi. This large value is added to the prior pressure inputs and the **PTA-APP-01B** run is repeated. Results lead to the same $k_{eff.}$ In summary, a long tube with a transducer located at the distant end (1) does not reduce permeability accuracy, (2) does not affect pressure inputs interpreted by the inverse algorithm, and (3) improves accuracy and resolution by widening the time measurement window. All three are welcome and positive.

Our algorithms and workflow were structured to produce the following results. First, the general boundary value problem applies only at the needle orifice and tissue beyond. The flow rate specification does not depend on *how* that rate is produced – it simply states the rate at the needle and circumvents any need for mechanical details. Thus, physical interpretations for **FT-00** are simple. At the start of injection, the fluid pushes hard and pressures must increase; when injections stop, pressures must decline. Now suppose we add a long fluid column to the syringe body. If the injection rate is constant and does not accelerate, significant dynamic effects are not introduced. However, power is added and required to push the column, leading to a constant pressure differential needed to overcome wall friction. But this constant does not affect the syringe boundary condition, one which depends on the $\partial P/\partial t$ term. The separate tissue and syringe math formulations used bypass mechanical details and related simulation complexities while leaving the physics accurately described. In addition, constant rate pumping simplifies the electrical control of auto-injection and infusion pumps.

Corrections where tubular pressure drops are subtracted from total pressure measured [3] *are* important in determining absolute pain thresholds. But as explained, whether or not the subtraction is performed does not affect predictions for permeability. The effect produced by longer flowlines does increase compressibility, which widens the time measurement window, a desirable effect – but without affecting the permeability. This widening was an unintended consequence of the two laboratory setups. For their authors' purposes, large time windows were not needed since only rapidly achievable steady plateau values for patient pain assessment were needed. However, in our work, which extracts information from dynamically changing pressure curves, larger time windows are important as they broaden the selection of pressure data input points available for inverse calculations. Again, it is not necessary to subtract flowline pressures from total pressures for inverse problems. There is no penalty in lengthening the flow line for window amplification purposes. In fact, depending on anticipated injectate compressibilities, optimal windows can be tuned using **FT-00** and **PTA-APP-01B** for optimal tube lengths.

We emphasize that increases in the product VC will widen time measurement windows, but it is not necessary to use long liquid filled tubes. In fact, a slightly longer syringe containing compressible gas, separated from the injectate by a movable flexible membrane, would accomplish the same result with greater syringe portability. This follows because gases are a hundred-fold more compressible than liquids. A convenient, non-toxic, readily available gas is room air. A one-way check valve and filter can be installed in-line so that, like a simple bicycle pump, clean room air enters from the outside to enhance system compressibility.

In pain threshold studies where the interest is in steady plateau pressures values themselves, flowline pressure subtraction is essential. However, this does not require separate "in air" tests used in recent investigations [3]. Required tubular pressure drops can be obtained from conventional pipe flow formulas for Newtonian, Power Law, Bingham Plastic and Herschel-Bulkley rheologies. Such equations apply to laminar (and not turbulent) flows, but steady conditions are almost always met in syringe applications. Finally, we describe final Run 3 results, where V is reduced to a reasonable 100 cc, with equilibration time decreasing to 6 sec. From this transient history, we select pressures at 0, 2 and 4 sec, again adding a 1,000 psi fictitious pressure drop, for inverse **PTA-APP-01B** analysis. As expected, we predict a 26.55 md effective permeability. The transient Darcy pressure due to tissue response simply adds to a dynamically insignificant background pressure, just as acoustic sound is unaffected by the presence of a variable wind.

Discussion and Closing Remarks

Methods predicting permeability, anisotropy, compressibility, porosity and background pressure from syringe pressure transients were developed. The inverse results, requiring three (time, pressure) points along buildup or drawdown curves, were validated using self-consistent forward-inverse procedures. Individual k_h and k_v values can also be found knowing $k_h^{2/3}k_v^{1/3}$ from buildup or drawdown tests, plus time delay "needle point to external probe" measurements, versus the timewise lengthier but simpler steady approach described here. More details, clinical applications, and forward and inverse models appear in

Biofluids Modeling, a recent 2023 book from John Wiley & Sons [8]. The present paper builds upon a ResearchSquare preprint published earlier in [9]. Altogether, the methods are useful in providing rapid, quantitative, minimally invasive and accurate local descriptions for tissue characterization. They can be used in understanding physical anomalies, in convenient periodic monitoring and, for example, in acupuncture research focused on the role of activation and deactivation of biological switches in living human and animal tissue.

Windows software modules **FT-00, FT-01, FT-PTA-01B, FT-PTA-DDBU** and **POROSITY** are available on request from the authors. Six research monographs developing the present methodology for geoscience applications are available from John Wiley & Sons and Elsevier Scientific Publishing. These books are also available from www.amazon.com using author search parameters "Wilson Chin" and "Wilson C. Chin." In this paper, our methodologies were illustrated using human and Yorkshire swine pressure transient data in [2,3], respectively. We emphasize that we did *not* perform any human or live animal experiments so that related regulatory procedures are not applicable. It is worth noting that the pressure versus time curves studied are similar in shape to those normally encountered in geoscience porous media flow applications. This confirms our view that syringe induced effects in tissue represent analogous porous media flow phenomena in rocks.

Data Availability

All data generated or analyzed during this study are included in this published article. Software derivations, discussions and availability are discussed under "Methods for Pressure Interpretation."

Acknowledgements

An un-reviewed pre-print version of the present paper was published earlier online, entitled "Intelligent Syringe for Porous Tissue Characterization Using Advanced Darcy Flow Pressure Transient Analysis," by W.C. Chin, J.A. Chin and X. Zhuang. Publication details are listed under "References" in Item [9].

Funding Information and Conflicts of Interest

Research and development was entirely supported by Stratamagnetic Software, LLC internal funding. The twenty-year-old private enterprise, wholly owned by the authors, has recently applied for "Intelligent Syringe" intellectual property protection. No other conflicts of interest are noted.

Author Contributions

The first author earned his Ph.D. at M.I.T. and M.Sc. at Caltech in fluid mechanics, physics and applied math. W.C.C. developed the theory, validations and method, and wrote the manuscript. J.A.C. performed simulations for syringe tubular extension versus supplemental gas substitution for time window amplification. Finally X.Z. evaluated possible transducer layouts for permeability and anisotropy prediction.

References

1. Abramowitz M and Stegun IA. *Handbook of Mathematical Functions.* (1970).
2. Woodley WD, Morel DR, Sutter DE, Pettis RJ and Bolick NG. Clinical evaluation of large volume subcutaneous injection tissue effects, pain, and acceptability in healthy adults. *Clinical and Translational Science*. 15 (2022): 92-104.
3. Doughty DV, Clawson CZ, Lambert W and Anand Subramony J. Understanding Subcutaneous Tissue Pressure for Engineering Injection Devices for Large-Volume Protein Delivery. *Journal of Pharmaceutical Sciences*. 105 (2016): 2105-2113.
4. Duran-Reynals F. Tissue Permeability and the Spreading Factors in Infection. *Bacteriol Rev* 6 (1942): 197-252 (1942).
5. Yuan SY and Rigor RR. *Regulation of Endothelial Barrier Function*, *Chapter 3 – Methods for Measuring Permeability*. Morgan & Claypool Life Sciences (2010).
6. Claesson-Welsh L, Dejana E and McDonald D. Permeability of the endothelial barrier: identifying and reconciling controversies. *Trends Mol Med* 27 (2021): 314–331.
7. Baish JW, Padera TP and Munn LL. The effects of gravity and compression on interstitial fluid transport in the lower limb. *Nature, Scientific Reports*. Article 4890 (2022).
8. Chin WC and Chin JA, *Biofluids Modeling – Methods, Perspectives and Solutions*. John Wiley & Sons, (2023).
9. Chin WC, Chin JA and Zhuang X. "Intelligent Syringe for Porous Tissue Characterization Using Advanced Darcy Flow Pressure Transient Analysis," with preprint appearing on Research Square website under Internet link, https://assets.researchsquare.com/files/rs-3029461/v1_covered_7a041629-67e4-4b37-8db0-adeaf5303a82.pdf?c=1694088447, July 18, 2023.